THE ASTROPHYSICAL JOURNAL, 404:441–450, 1993 February 20

MAPPING THE DARK MATTER WITH WEAK GRAVITATIONAL LENSING

NICK KAISER AND GORDON SQUIRES
CIAR Cosmology Programme, CITA, University of Toronto, 60 St. George Street, Toronto, Ontario, Canada M5S 1A7
Received 1992 May 12; accepted 1992 August 18

ABSTRACT

We consider the problem of reconstructing the projected mass distribution in clusters from coherent distortions of background galaxies. The ellipticity of a background galaxy provides an estimate of the trace-free components of the tidal field $\partial^2\Phi/\partial\theta_i\,\partial\theta_j$ where $\Phi(\theta)$ is the two-dimensional potential generated by the surface density $\Sigma(\theta)$. We present a technique for inverting this problem. The resulting surface density contains a strong, but incoherent, random component arising from the random intrinsic galaxy ellipticities. This can be removed by filtering. Our method is very similar in form to that of Tyson et al., and the latter is given a rigorous interpretation as a particular implementation of filtering. We present simulations to illustrate the application of the method.

Subject headings: cosmology: theory — dark matter — gravitational lensing

1. INTRODUCTION

We view distant galaxies through an imperfect medium; the light from distant objects propagates to us as it would through a piece of glass with spatially inhomogeneous refractive index $e(\boldsymbol{r}) = 1 - 2\phi(\boldsymbol{r})$, where $\phi(\boldsymbol{r})$ is the Newtonian potential arising from density fluctuations, and this causes the images of distant galaxies to appear distorted. In an rms sense the distortions are small—probably less than a few percent on all angular scales—but are potentially detectable statistically. A particularly promising place to look for these distortions is behind dense foreground objects and Tyson, Valdes, & Wenk (1990, hereafter TVW) have shown that the galaxies behind rich clusters of galaxies are indeed measurably distorted.

The presence of dark matter in clusters is vividly revealed by the giant arcs (Lynds & Petrosian 1986; Soucail et al. 1987), and these observations provide powerful constraints on the mass distribution in the dense central parts of clusters (Hammer 1991). What TVW have done is rather different; they searched for weak distortion of the general background galaxy population and met with considerable success. Their study clearly shows the presence of copious amounts of dark matter, and they attempted to construct maps of the mass surface density (see also Tyson 1991). One exciting prospect is the possibility of extending this kind of analysis to map out the mass distribution in the outer parts of clusters. We know that in the populous parts of clusters the mass-to-light ratio is $\simeq 300\,h$ (e.g., Kent & Gunn 1982). While this is very large by comparison with the luminous parts of galaxies, it is still considerably less than that required to close the universe. It is quite possible that our estimates of M/L have been biased downwards because the galaxies are more centrally concentrated within the cluster than the dark mass (Carlberg & Dubinski 1991) and it would be very valuable to know if this is indeed the case. Another interesting prospect is to map out the mass in and around giant "walls" seen edge on. Although the distortions from these extended mass concentrations are small, they are still potentially measurable. For example, for a structure with radial density profile $\rho \propto 1/r^2$, the gravitationally induced ellipticity falls as $e \propto 1/\theta$, but the number of background galaxies rises as $N \propto \theta^2$, so the signal-to-noise ratio $\sim e/(N)^{1/2}$ is independent of scale (Miralda-Escude 1991), although of course it takes more telescope time to survey larger angles.

Kochanek (1990) and Miralda-Escude (1991) have considered the problem of determining the position and mass or velocity dispersion of clusters from this kind of data by model fitting. Here we seek a model-independent reconstruction technique. The problem is the following: given a catalog of galaxies with shape parameters, such as FOCAS or APM quadrupole moments, we wish to solve for the projected mass density. A solution to this problem in Fourier space has been given by Kaiser (1992); here we formulate the solution in real space. This gives a practically useful algorithm and also a rigorous interpretation of the method of TVW.

2. METHOD

We first formulate the inversion assuming we are supplied with continuous fields describing the distortion of background galaxies; this would be applicable in the idealized limit of infinitely high surface density of background galaxies. In § 2.2 we convert this into a practical estimator; we find that the idealized estimator, while giving a fair estimate of the surface density, has formally infinite noise arising from the random intrinsic galaxy ellipticities. This noise can be made finite by filtering. In § 2.3 we show that the method of TVW can be interpreted as a particular form of filter and that their results are more accurately interpreted as a map of the surface potential $\Phi(\theta)$ rather than of $\Sigma(\theta)$.

2.1. *Idealized Analysis*

Gravitational lensing is a surface brightness conserving mapping

$$\mathscr{I}'(\theta) = \mathscr{I}(\theta - \nabla\Phi)\,, \tag{2.1.1}$$

where $\mathscr{I}'$ and $\mathscr{I}$ are the observed and intrinsic surface brightness patterns and where the potential Φ satisfies the two-dimensional Poisson's equation

$$\nabla^2\Phi = -\Sigma\,. \tag{2.1.2}$$

The source term $\Sigma(\theta)$ is the physical projected surface density measured in units of one-half of the critical value $\Sigma \equiv 2\Sigma_{\rm phys}/\Sigma_{\rm crit}$ (Blandford & Narayan 1986). If the lens and galaxy

lie at comoving distances w_l and w_g, respectively, then the critical surface density is

$$\Sigma_{\rm crit}(w_l, \omega_g)^{-1} = 4\pi G a(w_l) w_l (1 - w_l/w_g) , \qquad (2.1.3)$$

where, for an Einstein–de Sitter universe, the scale factor is $a(\eta) = \eta^2$ with $\eta_0 = 1$ and $a_0 = 2/H_0 = 6000$ Mpc h^{-1}. The comoving distance is $w = 1 - \eta$ and is related to redshift by $w = 1 - (1 + z)^{-1/2}$.

Let us assume we have identified galaxies and measured their quadrupole moments $Q'_{ij} = \int d^2\theta \theta_i \theta_j \mathscr{I}'(\theta)$, where the angles are measured relative to the centroid of the image. If we assume that $\Phi_{ij} = \partial^2\Phi/\partial\theta_i\,\partial\theta_j$ is coherent over a galaxy image then $\mathscr{I}'(\theta_i) = \mathscr{I}(\mathscr{D}_{ij}\theta_j)$, where $\mathscr{D}_{ij} = \delta_{ij} + \Phi_{ij}$, and the quadrupole moments transform as

$$Q'_{ij} = \mathscr{D}_{il}^{-1}\mathscr{D}_{jm}^{-1} \det(\mathscr{D})^{-1} Q_{lm} . \qquad (2.1.4)$$

If we rotate into the frame in which $\mathscr{D}_{ij}$ and Φ_{ij} are diagonal then $Q'_{ij} = Q_{ij}/\lambda_1\lambda_2\lambda_i\lambda_j$ where λ_1, λ_2 are the eigenvalues of $\mathscr{D}$. If we define the ellipticity parameters (Valdes, Tyson, & Jarvis 1983)

$$\begin{pmatrix} e_1 \\ e_2 \end{pmatrix} = \begin{bmatrix} (Q_{11} - Q_{22})/(Q_{11} + Q_{22}) \\ 2Q_{12}/(Q_{11} + Q_{22}) \end{bmatrix} \qquad (2.1.5)$$

then, to first order in Φ_{ij}, the effect of lensing is to transform these according to

$$\begin{pmatrix} e'_1 \\ e'_2 \end{pmatrix} = \begin{pmatrix} e_1 \\ e_2 \end{pmatrix} - (\Phi_{11} - \Phi_{22}) \begin{pmatrix} 1 - e_1^2 \\ e_1 e_2 \end{pmatrix} \qquad (2.1.6)$$

(Miralda-Escude 1991). The intrinsic distribution of background galaxies on the e_1, e_2 plane is symmetric about the origin, so $\langle e_1\rangle = \langle e_2\rangle = \langle e_1 e_2\rangle = 0$, and hence $\langle e'_1\rangle = -(\Phi_{11} - \Phi_{22})(1 - \langle e^2\rangle/2)$, $\langle e'_2\rangle = 0$. Thus, the expectation value of the ellipticity of a galaxy is proportional to the trace-free part of Φ_{ij}. The factor $1 - \langle e^2\rangle/2$ can be estimated from the observed ellipticity distribution. For realistic ellipticity distributions it is close to unity and rather insensitive to the details of the distribution, and we will assume that it has been absorbed into the estimated ellipticities as a correction. Finally then, in a general coordinate frame, we find

$$\langle e'_i\rangle = D_i\Phi , \qquad (2.1.7)$$

where

$$\begin{pmatrix} D_1 \\ D_2 \end{pmatrix} = \begin{pmatrix} \partial^2/\partial\theta_1\,\partial\theta_1 - \partial^2/\partial\theta_2\,\partial\theta_2 \\ 2\partial^2/\partial\theta_1\,\partial\theta_2 \end{pmatrix} . \qquad (2.1.8)$$

The two-component quantity e_i is a "polar" (Blandford et al. 1991)—it transforms under rotation as $e'_i = R_{ij}(2\psi)e_j$—and it measures the stretching of galaxy images along and diagonal to the coordinate axes. The advantage of this description is that the e_i are linear in the potential Φ, so we can average together estimates of e_i to beat down the noise from the random intrinsic ellipticities.

From equations (2.1.7), (2.1.2), and ignoring for the moment the random intrinsic ellipticity, we have

$$e_i(\boldsymbol{\theta}) = -D_i\nabla^{-2}\Sigma(\boldsymbol{\theta}) , \qquad (2.1.9)$$

where the symbol ∇^{-2} denotes the inverse of the Laplacian operator. This is readily inverted in Fourier space. If we define $\tilde{e}_1(\boldsymbol{\kappa}) = \int d^2\theta e_i(\boldsymbol{\theta}) \exp(i\boldsymbol{\kappa}\cdot\boldsymbol{\theta})$, etc., then we have

$$\tilde{e}_i(\boldsymbol{\kappa}) = -\chi_i(\boldsymbol{\kappa})\tilde{\Sigma}(\boldsymbol{\kappa}) , \qquad (2.1.10)$$

where the operator $D_i\nabla^{-2}$ has become the algebraic function

$$\chi_i(\boldsymbol{\kappa}) \equiv \begin{bmatrix} (\kappa_1^2 - \kappa_2^2)/\kappa^2 \\ 2\kappa_1\kappa_2/\kappa^2 \end{bmatrix} . \qquad (2.1.11)$$

From equation (2.1.10) we see that either $\tilde{e}_1(\boldsymbol{\kappa})/\chi_1(\boldsymbol{\kappa})$ or $\tilde{e}_2(\boldsymbol{\kappa})/\chi_2(\boldsymbol{\kappa})$ would, in principle, suffice to give an estimate of $\tilde{\Sigma}(\boldsymbol{\kappa})$—which could then be inverse transformed to give $\Sigma(\boldsymbol{\theta})$—and the optimal linear combination of these is

$$\tilde{\Sigma}(\boldsymbol{\kappa}) = -\chi_i(\boldsymbol{\kappa})\tilde{e}_i(\boldsymbol{\kappa}) \qquad (2.1.12)$$

(Kaiser 1992).

If we Fourier transform equation (2.1.12) we will obtain an expression for $\Sigma(\boldsymbol{\theta})$ as a convolution of $e_i(\boldsymbol{\theta})$ with a kernel which is just the Fourier transform of $\chi_i(\boldsymbol{\kappa})$. A simple way to the desired result is to note that in real space, the operator representation of equation (2.1.12) is

$$\Sigma(\boldsymbol{\theta}) = -D_i\nabla^{-2}e_i(\boldsymbol{\theta}) . \qquad (2.1.13)$$

We can write down $\nabla^{-2}e_i$; it is the "potential" generated by a source $e_i(\boldsymbol{\theta})$:

$$\nabla^{-2}e_i(\boldsymbol{\theta}) = \frac{1}{2\pi}\int d^2\theta' \epsilon_i(\boldsymbol{\theta}') \ln|\boldsymbol{\theta}' - \boldsymbol{\theta}| , \qquad (2.1.14)$$

and applying the differential operator D_i to this we obtain

$$\Sigma(\boldsymbol{\theta}) = -\frac{2}{\pi}\int d^2\theta' \frac{\chi_i(\boldsymbol{\theta}' - \boldsymbol{\theta})e_i(\boldsymbol{\theta}')}{(\boldsymbol{\theta}' - \boldsymbol{\theta})^2} . \qquad (2.1.15)$$

Of course, we could have just Fourier transformed $\chi_i(\boldsymbol{\kappa})$ to obtain $\tilde{\chi}_i(\boldsymbol{\theta}) = 2\chi_i(\boldsymbol{\theta})/\pi\theta^2$, and then equation (2.1.15) follows from equation (2.1.12) from the convolution theorem. The steps above provide a simple way to perform the transform (see Hamilton 1992 for a similar application).

In polar coordinates, the kernel $\chi_i(\boldsymbol{\theta})/\theta^2$ appearing in equation (2.1.15) is $[\cos(2\psi)/\theta^2, \sin(2\psi)/\theta^2]$ which is, modulo a constant, just (minus) the ellipticity pattern produced by a point mass. Thus equation (2.1.15) has a simple graphical interpretation: to calculate the mass at some position $\boldsymbol{\theta}$ we must take the polar "dot" product of $e_i(\boldsymbol{\theta})$ with the ellipticity pattern from a point mass at $\boldsymbol{\theta}$ and then integrate over space. It is, of course, very plausible that something like this would correlate with the surface density—if we sit on a dense blob of mass then the observed ellipticity pattern should match the "template" $\chi_i(\boldsymbol{\theta})/\theta^2$, and so we would expect a strong signal—what is less obvious is that this prescription is, in the absence of noise, exact. It is interesting to note that, from equation (2.1.9), the ellipticity is obtained from the surface density by applying the operator $D_i\nabla^{-2}$ and then, from equation (2.1.13), the surface density is recovered by applying the same operator again. To prove the method we need only show that the contraction of $D_i\nabla^{-2}$ with itself is the unit operator. This is straightforward since from the definition of D_i (eq. [2.1.8]) we find $D_iD_i = (\nabla^2)^2$. Similarly, in Fourier space, we readily find that $\chi_i(\boldsymbol{\kappa})\chi_i(\boldsymbol{\kappa}) = 1$, but as noted, in the integral representation (eq. [2.1.15]) the corresponding identity is not so obvious.

In the foregoing analysis we assumed that the galaxies were all at a single distance w_g, whereas in reality the galaxies have some distribution of distances dn/dw_g. This is readily incorporated in the above formalism if we define the average inverse critical surface density,

$$\Sigma_{\rm crit}^{-1}(\omega_l) = 4\pi G a(w_l) w_l \frac{\int_{w_l}^{\infty} dw_g\, dn/dw_g (1 - w_l/w_g)}{\int_0^{\infty} dw_g\, dn/dw_g} , \qquad (2.1.16)$$

and use $\Sigma_{\rm crit}(w_l)$ in place of $\Sigma_{\rm crit}(w_l, w_g)$.

Another possible modification is to use some other estimate of the shape of a galaxy in place of the ellipticity parameters defined in equation (2.1.5). There are many possible alternatives which would give a linear estimate of $\Phi_{11}-\Phi_{22}$ as in equation (2.1.6). There are various factors to consider in choosing an estimator. These include: (1) How large are the second order (in Φ) corrections to equation (2.1.6)? (2) How large is the statistical uncertainty in the quantity measured? (3) How sensitive is the estimator to the form of the intrinsic ellipticity distribution? For instance, Kochanek (1991) has suggested that one use the "orientation matrix" which in our notation corresponds to using $e_i/|e|$ as the estimator rather than e_i. Kochanek's estimator has the advantage that it is independent of the atmospheric seeing—which will tend to circularize images—but only in the limit that the instrumental noise in the image is negligible. Miralda-Escude (1991) has shown that on points 1 and 3 above this estimator performs rather poorly (see his Figs. 2*a* and 7*b*) compared to the straight average of e_i, and there is also a penalty in the statistical uncertainty (at least if the intrinsic ellipticity distribution is assumed to be Gaussian). In our opinion equation (2.1.5) seems quite satisfactory.

Equation (2.1.6) is strictly valid only for weak distortions $\langle e_i\rangle \ll 1$. In general, $\langle e_1'\rangle$ is a function of λ_1/λ_2, the ratio of the eigenvalues $\mathscr{D}_{ij}$, with the functional form depending on the distribution of intrinsic ellipticities. At the Einstein radius $\lambda_2 \to 0$, and we find $e_1' = -1$; corresponding to an infinitely stretched image. It is interesting to note that for an isothermal sphere, we have $\Phi_{11} = 0$, so for sources on the Einstein radius we have $e_1 = \Phi_{11}-\Phi_{22}$, so, aside from the factor $1 - \langle e^2\rangle/2$, the weak lensing analysis is valid even in this highly nonlinear situation.

2.2. *Practical Estimator*

So far, we have thought of $e_i(\boldsymbol{\theta})$ as a continuous polar field. In reality, we are supplied with a set of samples of $e_i(\boldsymbol{\theta})$ at the random locations of the background galaxies, plus, of course, a random intrinsic ellipticity for each galaxy. Given a catalog of background galaxies one could bin these on a grid and define e_i for a cell to be the average or median ellipticity for the galaxies enclosed and then perform the convolution of equation (2.1.15) on the grid. Alternatively one can convert this to a sum over galaxies:

$$\hat{\Sigma}(\boldsymbol{\theta}) = -\frac{2}{\bar{n}\pi}\sum_{\text{galaxies}}\frac{\chi_i(\boldsymbol{\theta}_g-\boldsymbol{\theta})e_i}{(\boldsymbol{\theta}_g-\boldsymbol{\theta})^2}\,, \tag{2.2.1}$$

where $\bar{n}$ is the surface number density of background galaxies. Equation (2.2.1) is equivalent to a grid-based computation with a fine grid and with weight per cell proportional to the occupancy.

It is easy to show that $\langle\hat{\Sigma}(\boldsymbol{\theta})\rangle = \Sigma(\boldsymbol{\theta})$, but unfortunately the uncertainty $\langle(\hat{\Sigma}-\Sigma)^2\rangle$ is infinite. The Fourier transform of equation (2.2.1) is $\tilde{\Sigma}(\boldsymbol{\kappa}) = \bar{n}^{-1}\chi_i(\boldsymbol{\kappa})\sum e_i \exp(i\boldsymbol{\kappa}\cdot\boldsymbol{\theta})$. If we assume that the intrinsic ellipticities are statistically uncorrelated we find $\langle\tilde{\Sigma}(\boldsymbol{\kappa})\tilde{\Sigma}^*(\boldsymbol{\kappa})\rangle = \langle e^2\rangle/2\bar{n}$, where $\langle e^2\rangle$ is the mean square intrinsic ellipticity. The random intrinsic ellipticities introduce a white spectrum noise and consequently the contribution to $\langle\hat{\Sigma}(\boldsymbol{\theta})^2\rangle = (2\pi)^{-2}\int d^2\kappa\langle\tilde{\Sigma}^2(\boldsymbol{\kappa})\rangle$ diverges at high frequency. The problem can be cured by introducing a low-pass filter. If the transfer function for the filter is $T(k)$ then $\langle\Sigma(\boldsymbol{\theta})^2\rangle = \langle e^2\rangle\int d^2\kappa T^2(\kappa)/(8\pi^2\bar{n})$. For smoothing with a two-dimensional Gaussian filter $\propto \exp(-\theta^2/2\Theta^2)$, for instance, the transfer function is $T(\kappa) = \exp(-\kappa^2\Theta^2/2)$, and we have $\langle\Sigma^2(\boldsymbol{\theta})\rangle = \langle e^2\rangle/8\pi\bar{n}\Theta^2$. The uncertainty in the map of $\Sigma(\boldsymbol{\theta})$ is on the order of the rms galaxy ellipticity divided by the root of the number of galaxies within the smoothing window. This uncertainty can be made small, though, at the expense of spatial resolution.

This smoothing can either be done after the fact on the field $\hat{\Sigma}(\boldsymbol{\theta})$ given by equation (2.2.1) or can be incorporated directly in the estimator by replacing $2\chi_i(\boldsymbol{\theta})/\pi\theta^2$ [the Fourier transform of $\chi_i(\boldsymbol{\kappa})$] by the Fourier transform of $\chi_i(\boldsymbol{\kappa})T(\kappa)$. Thus, in place of equation (2.1.15), we have

$$\Sigma(\boldsymbol{\theta}) = \int d^2\theta' W(\boldsymbol{\theta}'-\boldsymbol{\theta})\chi_i(\boldsymbol{\theta}'-\boldsymbol{\theta})e_i(\boldsymbol{\theta}')\,, \tag{2.2.2}$$

or, in place of equation (2.2.1),

$$\hat{\Sigma}(\boldsymbol{\theta}) = \frac{1}{\bar{n}}\sum_{\text{galaxies}} W(\boldsymbol{\theta}_g-\boldsymbol{\theta})\chi_i(\boldsymbol{\theta}_g-\boldsymbol{\theta})e_i(\boldsymbol{\theta}_g) \tag{2.2.3}$$

where

$$W(\theta) = \int\frac{d^2\kappa}{(2\pi)^2}\,T(\kappa)J_2(\kappa\theta)\,. \tag{2.2.4}$$

For a simple low-pass filter, perhaps a Gaussian, the weight function falls as $1/\theta^2$ as before for large angles, but the divergence at small angles is suppressed.

Equation (2.2.3) can be used to map the mass distribution in individual clusters. However, only for very rich clusters is there a strong signal-to-noise ratio. Poorer clusters and individual galaxies will not give a significant detection, but by stacking the estimates of Σ for a collection of similar objects one can hope to measure the ensemble average mass profile.

2.3. *Interpretation of TVW Method*

In polar coordinates, $\chi_i(\boldsymbol{\theta})$ is $\{\cos 2\psi,\ \sin 2\psi\}$ so $\chi_i(\boldsymbol{\theta}_g-\boldsymbol{\theta})e_i(\boldsymbol{\theta}_g)$ is just (minus) the tangential alignment of the galaxy at $\boldsymbol{\theta}_g$ relative to the point $\boldsymbol{\theta}$, so our estimator of $\Sigma(\boldsymbol{\theta})$ (eq. [2.2.3]) can be stated as follows: "For each candidate center $\boldsymbol{\theta}$, for each galaxy calculate the tangential ellipticity (relative to $\boldsymbol{\theta}$) and sum these with weights given by equation (2.2.4)." Comparing with the definition of the algorithm of TVW we find that their method is a special case of equation (2.2.3), with $W(\theta)$ given by the Heaviside function $\Theta(\theta/\theta_{\max})$. The outer cutoff was taken to be $\theta_{\max} \simeq 1.^\circ 4$. This corresponds to a radius of 300 kpc h_{75}^{-1}. Inverting equation (2.2.4) we find that this corresponds to a transfer function

$$T(\kappa) \propto \int_0^{\theta_{\max}} d\theta\,\theta[2J_1(\kappa\theta)/\kappa\theta - J_0(k\theta)] \tag{2.3.1}$$

and find that their method returns a map of the surface density convolved with the point spread function (psf)

$$W_{2D}(\theta) \propto \int d\kappa\,\kappa T(\kappa)J_0(\kappa\theta)\,. \tag{2.3.2}$$

The transfer function is shown in Figure 1. It is strongly peaked around $\kappa \simeq 4/\theta_{\max}$ and so acts, to a crude approximation, as a band pass filter. At high frequencies $\kappa \gg 1/\theta_{\max}$ the wiggles are superposed on a general $1/\kappa^2$ trend, but $\Sigma(\boldsymbol{\kappa})/\kappa^2 = -\Phi(\boldsymbol{\kappa})$, so for fluctuations on scales $\ll\theta_{\max}$, the TVW statistic is proportional to the surface potential $\Phi(\boldsymbol{\theta})$.

The psf $W_{2D}(\theta)$ is shown in Figure 2; it is a Mexican hat of sorts. The psf is divergent at small θ, but only logarithmically so. The weight is distributed with radius as $dW/d\theta = 2\pi\theta W_{2D}(\theta)$ and this, shown as a dashed line, is regular at $\theta = 0$.

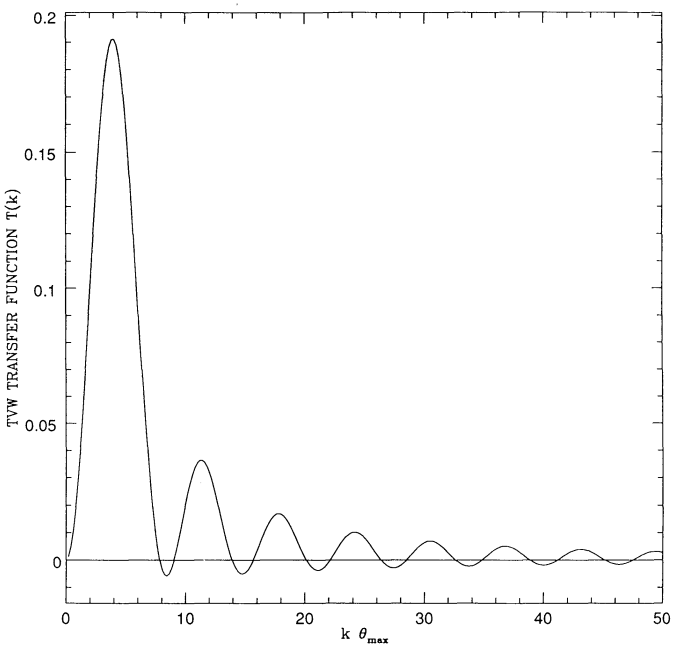

FIG. 1.—Transfer function for the TVW method obtained by evaluating eq. (2.3.1). There are wiggles arising from the sharp cutoff at θ_{max}. There is one dominant peak at $k \simeq 4/\theta_{max}$, and the response is strongly suppressed at higher and lower frequencies.

The psf is negative for $\theta \gtrsim 0.6\theta_{max}$ and the integrated weight—the area under the dashed curve—is zero. The TVW statistic can be best visualized as some average of the surface density within $0.6\theta_{max}$ minus the mean surface density determined in the annulus from $0.6\theta_{max}$ to θ_{max}. The response to a constant surface density is zero. This is very reasonable since a constant surface density produces no distortion. The zero net weight and circular symmetry give rise to the $T(k) \propto k^2$ asymptotic behavior for $k \ll \theta_{max}^{-1}$.

For A1689, the radial profile of the TVW statistic is shown in Figure 3. It shows a flat core rolling off at ~ 100 kpc h_{75}^{-1}. TVW calibrated the observed result against simulations using softened isothermal sphere clusters as lenses. They found that the observations constrained the velocity dispersion of the cluster but was insensitive to the core radius. This is illustrated in Figure 3 where we show the surface density for a family of such clusters. The dashed lines show the expectation for the TVW statistic. Even though the core radius varies by a factor 4 (from $\simeq 30$–120 kpc h_{75}^{-1}), the TVW statistic curves are barely distinguishable from each other or from the data. This behavior is easily understood in our interpretation of the TVW statistic as a measure of $\Phi(\theta)$. For a spherical cluster, $\Phi(\theta) = M(<\theta)\ln\theta$ + constant. In all the model clusters shown in Figure 3 the mass was a strongly increasing function of θ so $d\Phi/d\ln\theta$—the gradient of the curves in Figure 3—is very small at small radii. With these models the rollover at large θ is produced by the cutoff at θ_{max}. One might expect the TVW statistic to be a more powerful discriminator for mass models where a substantial fraction of the mass is found at small θ. An interesting example of such a distribution is given by the red light distribution for Abell 1689. A substantial fraction of the total light is apparently enclosed within 10 kpc or so of the cluster center, and outside of this the surface density falls roughly as θ^{-2}, so there is roughly equal light per log interval of angle. In Figure 4 we show the surface brightness profile and the prediction for the TVW statistic if the mass follows the light. As to be expected, the potential map is now much steeper in the center and the data disfavor this model.

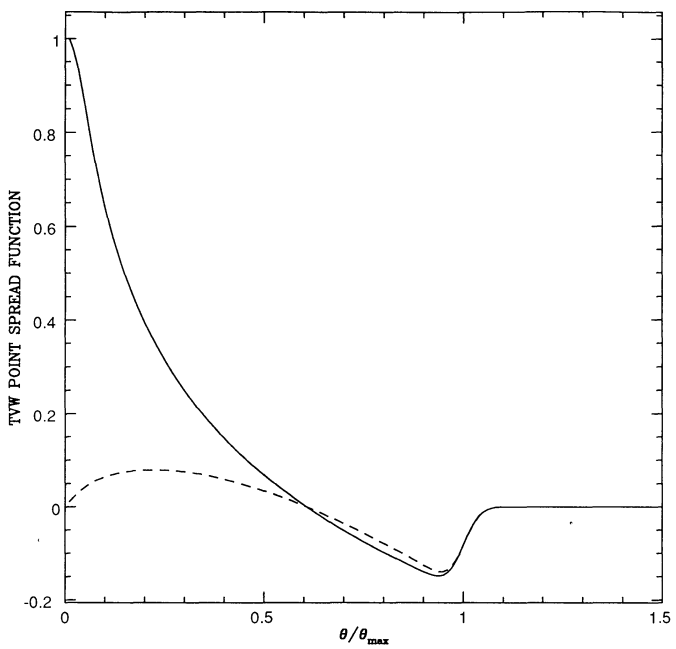

FIG. 2.—The solid curve is the point spread function for the TVW method obtained by applying eq. (2.3.2) to the transfer function shown in Fig. 1. To avoid ringing, the transfer function was attenuated by a factor $\exp(-\kappa^2/2\kappa_*^2)$ with $k_* = 50/\theta_{max}$. This renders the psf finite at $\theta = 0$. In reality it should be logarithmically divergent. The dashed line is the cumulant $\int d\theta\, \theta W_{2D}(\theta)$ and shows that spike at the origin makes a negligible contribution to the total weight.

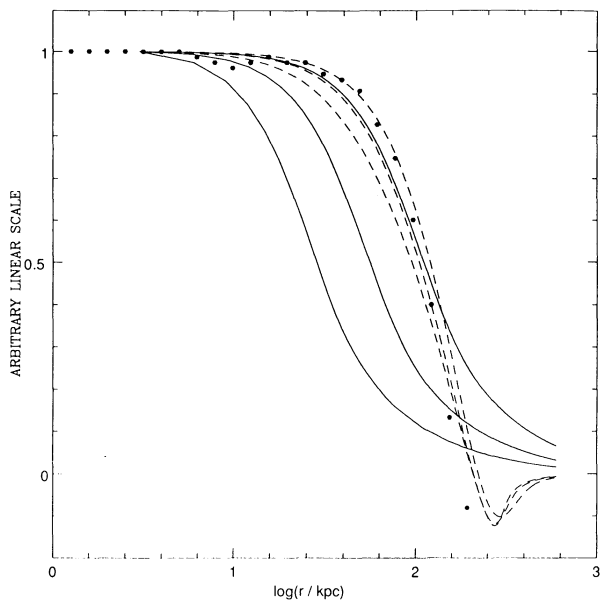

FIG. 3.—Solid lines are the projected surface density profiles for a family of softened isothermal sphere models with half-max core radii $r_c \simeq 30$, 60, and 120 kpc. Dashed lines are predictions for the reconstructed "surface density" using the method of TVW. Filled symbols are the actual estimate for Abell 1689 from TVW. All curves have been normalized to unity at small r and the scale corresponds to $H = 75$ for direct comparison with Fig. 4 of TVW. All the models provide a good fit to the data. The "shoulder" is best fit by the larger core radius.

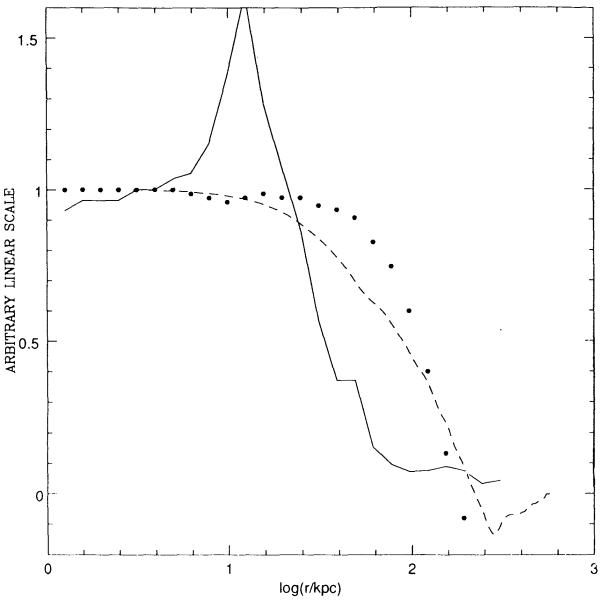

FIG. 4.—Solid line is the red light projected surface density profiles for A1689 from TVW. Dashed line is the prediction for the TVW surface density assuming the mass follows the red light. For this kind of mass distribution the surface potential is peakier than for the isothermal sphere models, and consequently the RVW estimate continues to rise below $r \simeq 100$ kpc. This is not seen in the data.

From the shape of the psf we infer that the value of the TVW statistic at the center of the cluster should give a reliable estimate of the mass contained within ~ 150 kpc of the cluster center, but is rather insensitive to details of the cluster mass profile. This problem can be anticipated from the transfer function (Fig. 1) which has one very prominent spike (at a scale set by the cutoff $\theta_{\rm max}$), and consequently the resulting maps are determined much more by the shape of the filter than the profile of the cluster. However, this is not a necessary limitation; with a minor modification to the algorithm one could obtain much higher spatial resolution. The price of higher angular resolution is increased noise, but it seems quite plausible that with these data one could distinguish between the models displayed in Figure 3.

3. SIMULATIONS

To see how well the method works in practice and explore some of the problems facing a practical application, we have made simulations by generating mock data for realistic model clusters.

The model adopted has a space density profile $\rho \propto 1/r^2$ at large radii with amplitude characterized by asymptotic velocity v for a circular orbit. The profile is softened in the center with a finite core radius. The critical surface density in physical units is

$$\Sigma_{\rm phys}(\theta) = v^2/[4Ga_l w_l(\sqrt{\theta^2 + \theta_{\rm core}^2})] , \qquad (3.1)$$

corresponding to a dimensionless surface density

$$\Sigma(\theta) = 2\Sigma_{\rm phys}(\theta)/\Sigma_{\rm crit} = 2\pi(1 - w_l/w_g)(v^2/c^2)(\theta^2 + \theta_{\rm core}^2)^{-1/2} . \qquad (3.2)$$

This model is a simple approximation to an isothermal sphere (e.g., Grossman & Narayan 1989). We have adopted a rotation velocity $v = 2100$ km s^{-1} as a benchmark; this corresponds to a one-dimensional velocity dispersion for the dark matter of 1500 km s^{-1}. If the galaxies are more condensed than the dark mass then they may have a considerably lower velocity dispersion. We take the core radius to be 0.12 Mpc h^{-1}, and we place the cluster at $z_l = 0.37$. At this redshift, the core radius subtends an angle $\theta_{\rm core} \simeq 0'.5$.

We assume that the background galaxies lie at $z_g = 1$. For this combination of redshifts $\langle 1 - w_l/w_g \rangle = 0.5$, and we find $\Sigma(\theta) \simeq (0/32'')^{-1}$ for $\theta \gg \theta_{\rm core}$. The tangential ellipticity is $e_T = \Sigma$, so the weak distortion approximation should be valid at angles greater than $\sim 0'.5$—roughly the angle subtended by the core radius in our benchmark model. The background galaxies were laid down with a uniform, random distribution on the sky with surface density $\bar{n} = 10^5$ per square degree as appropriate for a limiting blue magnitude of $m \simeq 26$ (Tyson & Seitzer 1988; Lilly, Cowie, & Gardner 1991). The positions of the galaxies were assumed to be uniformly distributed over observed rather than intrinsic positions. While strictly incorrect—we should have allowed for the displacement of the galaxies due to the lensing—the slope of the observed number counts $n(>l) \simeq l^{-1}$ are such that once allowance is also made for the amplification of the apparent luminosities the surface density of galaxies is essentially unperturbed.

The intrinsic quadrupole moments were generated to be

$$Q_{ij} = \begin{pmatrix} 1 & 0 \\ 0 & 1 \end{pmatrix} + e_1 \begin{pmatrix} 1 & 0 \\ 0 & -1 \end{pmatrix} + e_2 \begin{pmatrix} 0 & 1 \\ 1 & 0 \end{pmatrix} ,$$

where the ellipticity parameters e_1 and e_2 were drawn from Gaussian distributions with $\langle e^2 \rangle^{1/2} = (2)^{1/2} \langle e_i^2 \rangle^{1/2} = 0.3$. For each galaxy, we calculate the tidal field Φ_{ij} and then transform the Q_{ij} according to equation (2.1.4) to obtain the "observed" ellipticities. This process correctly distorts the galaxies even in the nonlinear regime and so provided a test of the robustness of the method to departures from linearity.

Our model clusters have smooth profiles. More realistically one might want to include a clumpy component associated with the galaxies. However, the ellipticities generated by the cluster galaxies are small for any angular separation greater than a few arcseconds, and since small distortions add linearly they may safely be ignored.

We show in Figures 5*a*–5*d* our simulation for a single, softened isothermal sphere model lens. The input foreground surface density is shown in Figure 5*a* with the cluster centered in a 15′ field. We have generated synthetic deep images with appropriately stretched but otherwise randomly oriented galaxies. The coherent tangential alignment generated by the lens is not immediately apparent. Even near the lens center, where the gravitational stretching is highest, the intrinsic ellipticities of the galaxies mask the gravitational signal. Figures 5*b*–5*c* show the surface density reconstructed from this ellipticity pattern according to equation (2.1.12). A low pass Gaussian filter was used to reduce the noise level with filter scale of 0′.25 and 1′, respectively. This filter scale can be tuned to highlight large or smaller scale structures.

We show the radially averaged reconstructed surface density in Figures 6*a*–6*b* for the softened isothermal sphere lens with rotation velocities of 1400 km s^{-1} and 2100 km s^{-1}, respectively. The solid line in the figures shows the input surface density; the points are the reconstruction at logarithmically increasing radii. The DC level in the reconstruction has been set so that the surface density is zero at the edge of the frame. This means the reconstructed points tend to fall below the

1993ApJ...404..441K

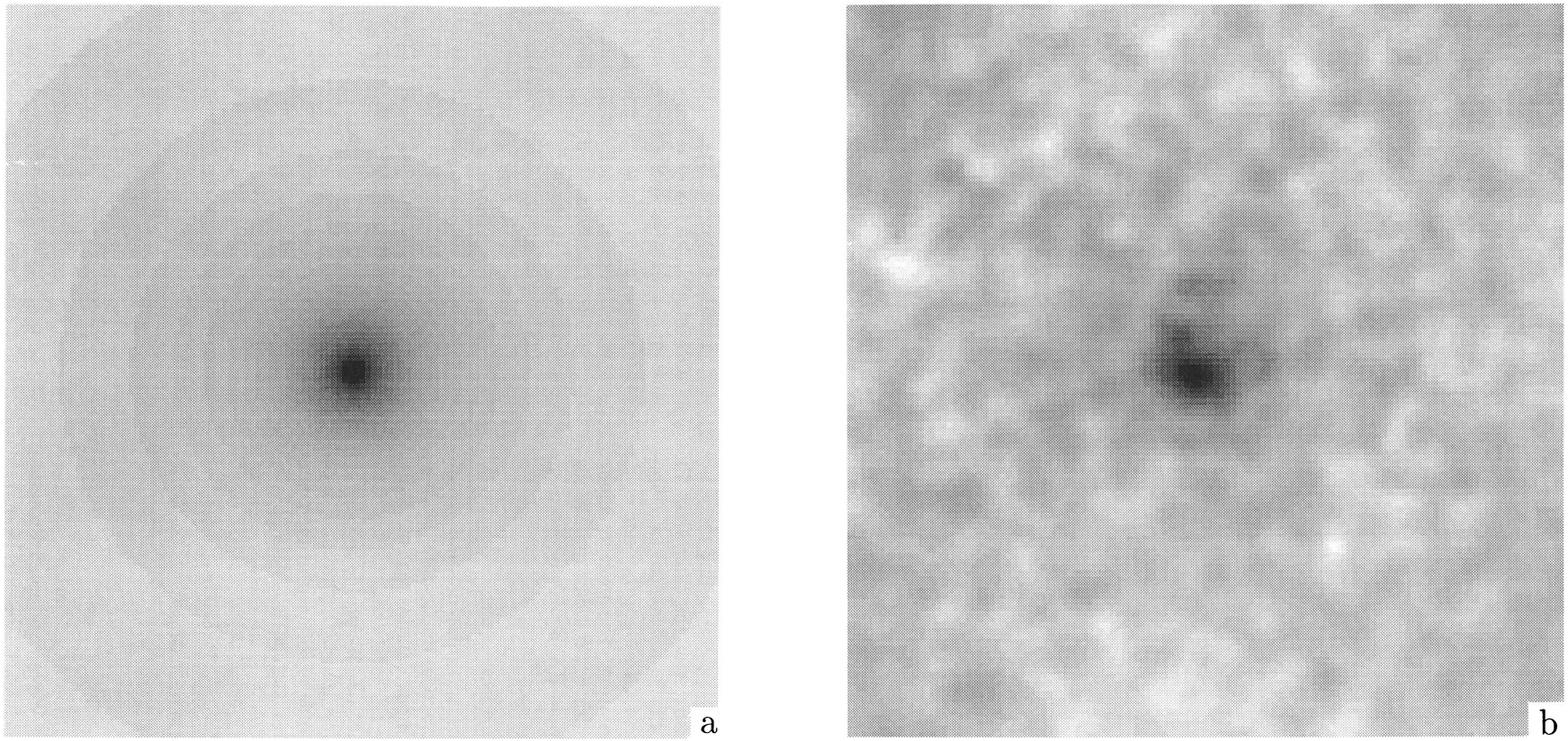

FIG. 5.—(*a–f*) The method has been tested using simulated background galaxies. (*a*) The input surface density. The cluster lens has rotation velocity $v = 2100$ km s^{-1} and a soft core of 0.12 Mpc or $\sim 0.'64$. Ellipticities were generated for 6000 background galaxies. While images of the background field revealed no distortion that was obvious to the eye, the software managed to reconstruct the density as shown in (*b*) and (*c*) for smoothing with Gaussian filters of $0.'25$ and $1'$, respectively. Panel (*d*) shows a double cluster with cluster centers separated by $3'$, and panels (*e*) and (*f*) show the reconstruction, again for two choices of smoothing radius.

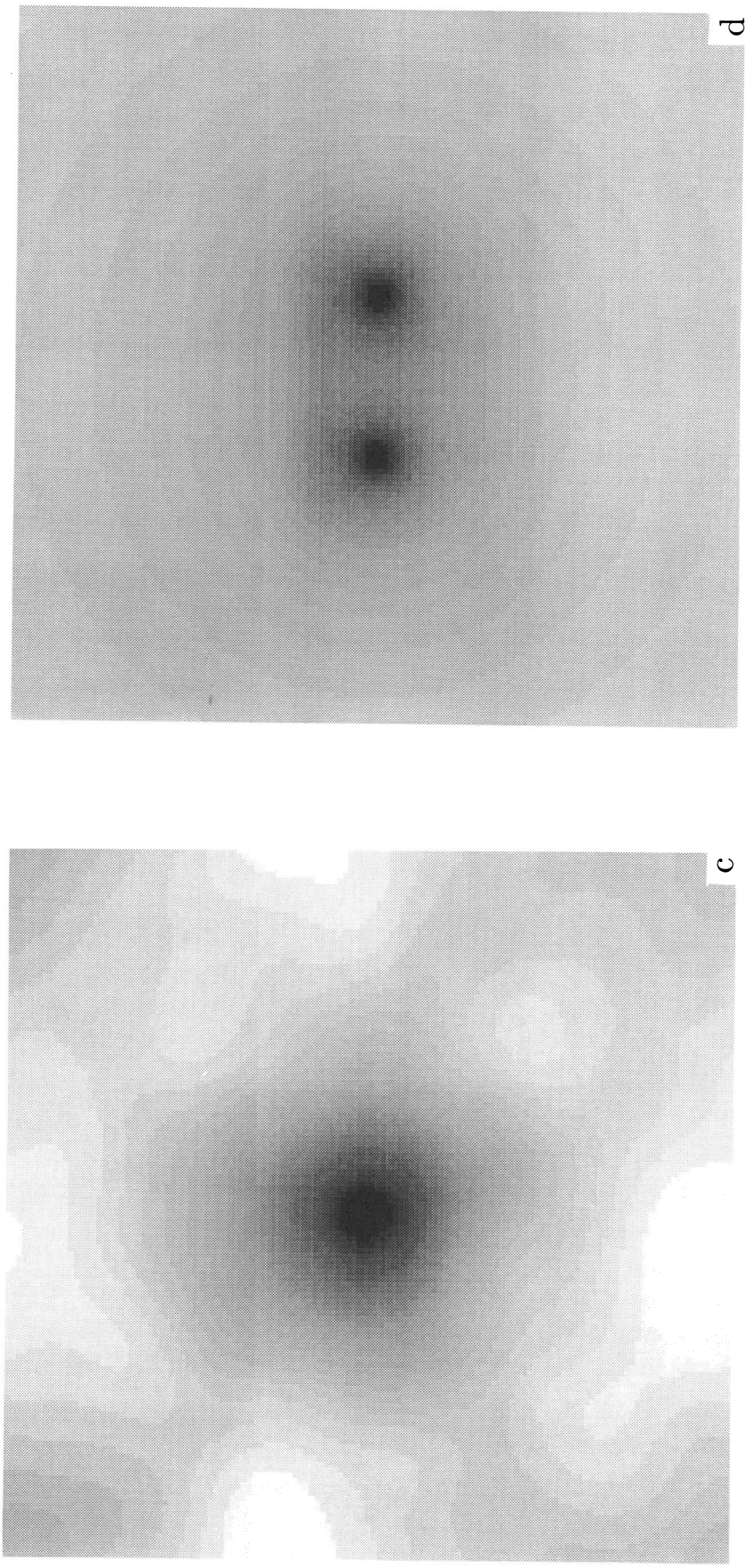

FIG. 5—*Continued*

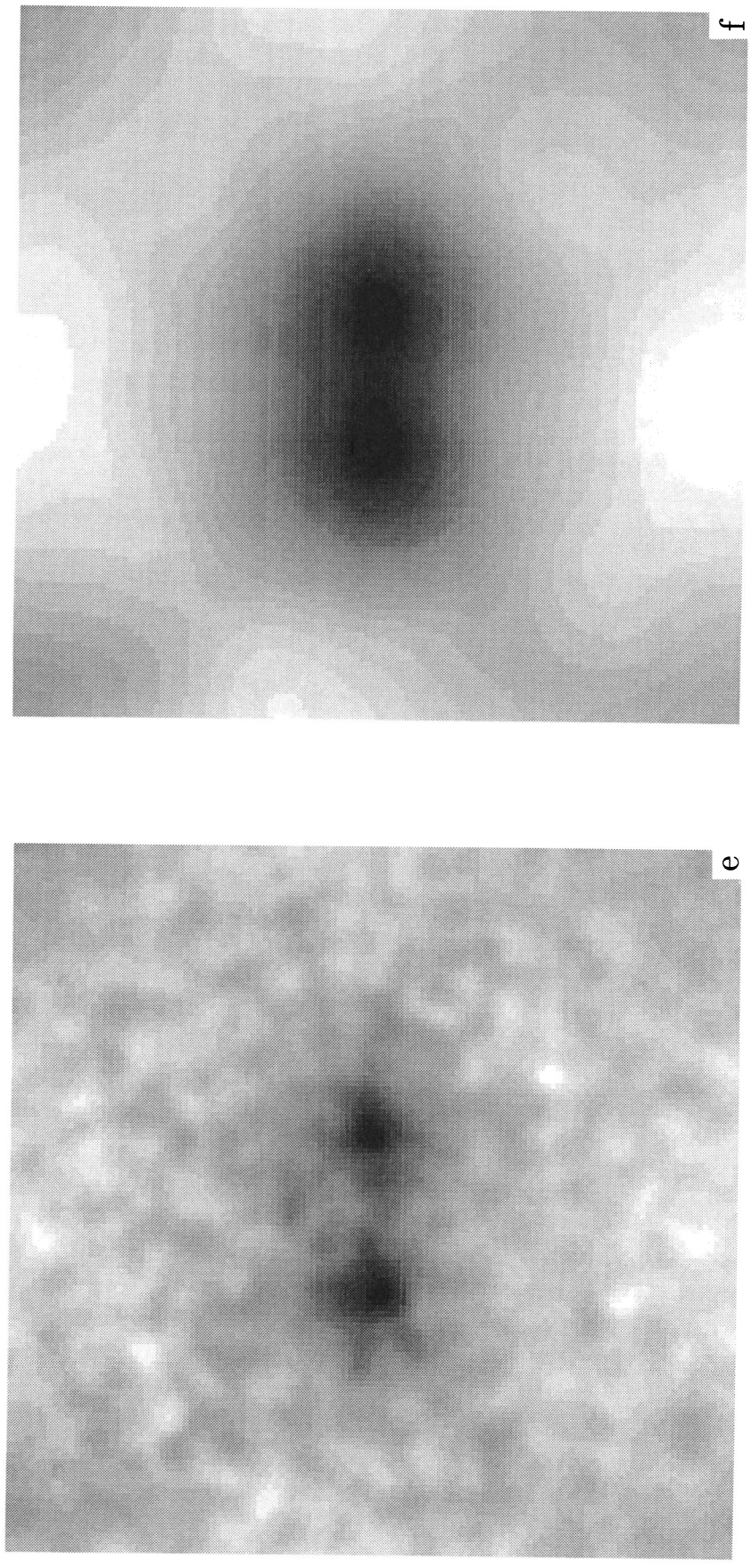

FIG. 5—*Continued*

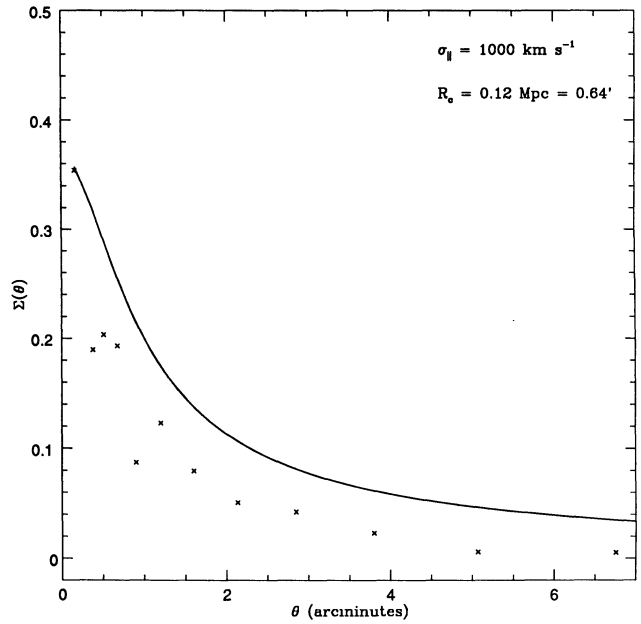

FIG. 6a

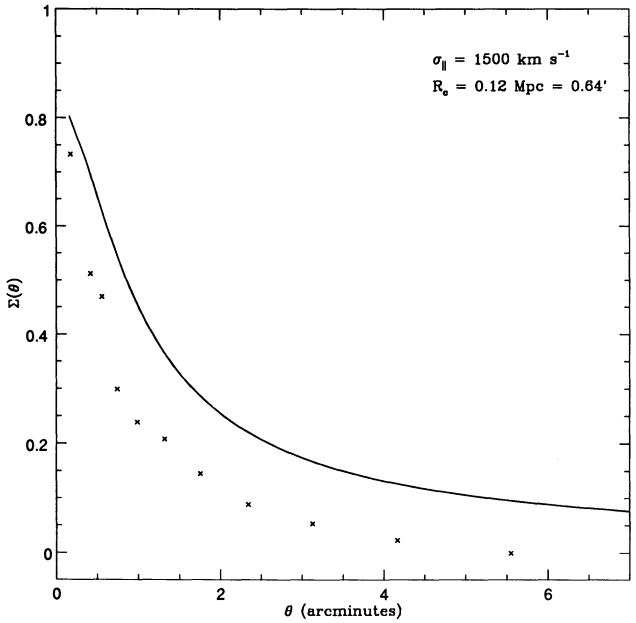

FIG. 6b

FIG. 6.—(*a–b*) The solid lines are the input surface density for a cluster with rotation velocity of 1400 and 2100 km s^{-1}, respectively. The points are the radially averaged, reconstructed surface density at logarithmically increasing radii. The DC level in the reconstruction is set so that the surface density is zero at the edge of the frame.

input density. However, the shape of the reconstruction matches the input surface density remarkably well. At small angles there tends to be more scatter in the reconstruction. This reflects the fact that fewer galaxies were used in the central regions for this reconstruction, so the statistics are poorer.

Figures 5*d*–5*f* show the results for a simulation of a pair of clusters. We have taken two clusters separated by 3.'3 on a 15' field. Each cluster was taken to be a softened isothermal sphere with the same core radius and rotation velocity as used for our single benchmark cluster. Figure 5*d* shows the input surface density and Figures 5*e*–5*f* show the reconstructed surface density for the choice of filter scales used in the single lens case. Again, both the broad and local features of the density profile are recovered by this technique.

This method of density reconstruction requires that the gravitational signal occurs in the weak regime. For a singular isothermal sphere, $e_T = \Sigma$ so that weak lensing requires that $\Sigma \ll 1$. For our benchmark clusters in Figures 6*a*–6*b*, this condition is satisfied. We now consider how our method will perform when we leave the weak lensing regime.

We have adopted the parameters used by Tyson (1991) for his simulation of A1689. We take a single cluster lens with a one-dimensional velocity dispersion of 1750 km s^{-1} and a core radius of 0.045 h^{-1} kpc. There are several features in this field that differ from the weak lensing simulations. There are giant arcs at $\sim$0.'7 from the cluster center; the Einstein radius for this cluster. Inside the Einstein ring, galaxies pass through the transition from extreme tangential elongation to zero-induced ellipticity to extreme radial elongation near the lens center.

In Figure 7 we show our reconstruction for the surface density for this lens. The solid line shows the input cluster surface density, and the points denote the radially averaged, reconstructed surface density at logarithmically increasing radii. Again, we have set the normalization so that the reconstructed density is zero at the edge of the frame. The Einstein radius corresponds to $\theta \sim 0.'7$ where $\Sigma = 1$. In the weak regime (outside the Einstein radius), we see that the reconstruction is quite good. Even in the strong regime, our method seems fairly robust. The innermost point is too low, but the number of galaxies within this radius is small so the significance of this point is slight. Thus, it seems that in the strong lensing regime, where our formalism is not strictly valid, the method is still

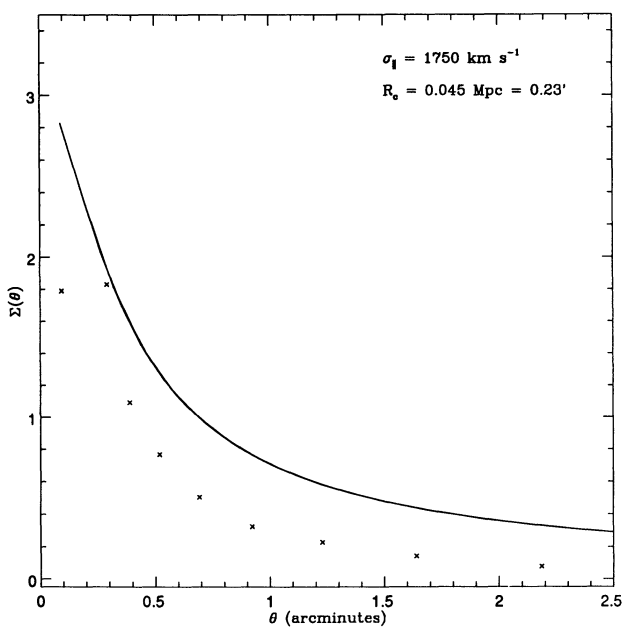

FIG. 7.—Simulation to explore the behavior of the method in the transition to the strong lensing regime. The cluster velocity dispersion and field size (5') were chosen to model the TVW observation of A1689. As in Fig. 6, aside from a constant shift due to the unknown DC surface density, the reconstruction recovers the shape quite well.

fairly robust. This may prove important if this is to be a viable method for determining the cluster core radius, for example.

4. SUMMARY

In § 2.1 we derived an inversion formula (eq. [2.1.15]) for reconstructing the surface density field from measurements of galaxy ellipticities. In § 2.2 we found that the uncertainty in this estimator is formally infinite but can be made finite by low-pass filtering. This resulted in the practical algorithm expressed in equations (2.2.3) and (2.2.4). In § 2.3 we showed that the TVW statistic may be interpreted as a specific choice of filter and that their method returns a map of the surface density convolved with the psf shown in Figure 2. The shape of the psf is such that small-scale features are suppressed by two powers of angular scale and the TVW statistic is most accurately interpreted as a map of the surface potential. In § 3 we have made simulations of the reconstruction process. We found that even in situations where the coherent distortions of the simulated galaxies are invisible to the eye, the algorithm is capable of recovering the surface density.

REFERENCES

Blandford, R., & Narayan, R. 1986, ApJ, 321, 658
Blandford, R. D., Saust, A. B., Brainerd, T., & Villumsen, J. V. 1991, MNRAS, 251, 600
Carlberg, R., & Dubinski, J. 1991, ApJ, 369, 13
Grossman, S., & Narayan, R. 1989, ApJ, 344, 637
Hamilton, A. 1992, ApJ, 385, L5
Hammer, F. 1991, ApJ, 383, 66
Kaiser, N. 1992, ApJ, 388, 272
Kent, S. M., & Gunn, J. E. 1982, AJ, 87, 945
Kochanek, C. 1990, MNRAS, 247, 135
Lilly, S. J., Cowie, L. L., & Gardner, J. P. 1991, ApJ, 369, 79
Lynds, R., & Petrosian, V. 1986, BAAS, 18, 1014
Miralda-Escude, J. 1991, ApJ, 370, 1
Soucail, G., Fort, B., Mellier, Y., & Picat, J. 1987, A&A, 191, L19
Tyson, J., in Proc. After The First 3 Minutes, ed. S. Holt (New York: AIP), 437
Tyson, J. A., & Seitzer, P. 1988, ApJ, 335, 552
Tyson, J., Valdes, F., & Wenk, R. 1990, ApJ, 349, L1 (TVW)
Valdes, F., Tyson, J., & Jarvis, J. 1983, ApJ, 271, 431